Biomed Microdevices (2015) 17:21
DOI 10.1007/s10544-015-9936-y

A reusable device for electrochemical applications of hydrogel supported black lipid membranes

Agnieszka Mech-Dorosz · Arto Heiskanen · Sania Bäckström · Mark Perry · Haseena B. Muhammad · Claus Hélix-Nielsen · Jenny Emnéus

Abstract Black lipid membranes (BLMs) are significant in studies of membrane transport, incorporated proteins/ion transporters, and hence in construction of biosensor devices. Although BLMs provide an accepted mimic of cellular membranes, they are inherently fragile. Techniques are developed to stabilize them, such as hydrogel supports. In this paper, we present a reusable device for studies on hydrogel supported (hs) BLMs. These are formed across an ethylene tetrafluoroethylene (ETFE) aperture array supported by the hydrogel, which is during *in situ* polymerization covalently "sandwiched" between the ETFE substrate and a gold electrode microchip, thus allowing direct electrochemical studies with the integrated working electrodes. Using electrochemical impedance spectroscopy (EIS), X-ray photoelectron spectroscopy and contact angle measurements, we demonstrate the optimized chemical modifications of the gold electrode microchips and plasma modification of the ETFE aperture arrays facilitating covalent "sandwiching" of the hydrogel. Both fluorescence microscopy and EIS were used to demonstrate the induced spontaneous thinning of a deposited lipid solution, leading to formation of stabilized hsBLMs on average in 10 min. The determined specific membrane capacitance and resistance were shown to vary in the range 0.31–0.49 μF/cm^2 and 45–65 kΩ cm^2, respectively, corresponding to partially solvent containing BLMs with an average life time of 60–80 min. The characterized hsBLM formation and devised equivalent circuit models lead to a schematic model to illustrate lipid molecule distribution in hydrogel-supported apertures. The functionality of stabilized hsBLMs and detection sensitivity of the platform were verified by monitoring the effect of the ion transporter valinomycin.

Keywords Hydrogel supported black lipid membrane · Covalent tethering of hydrogel · ETFE aperture array · Plasma modification of ETFE · Spontaneous thinning of lipid layer · Impedance spectroscopy

1 Introduction

Biomimetic lipid membranes can constitute a suitable environment for membrane spanning proteins (Castellana and Cremer 2006; Kim et al. 2012; Nielsen 2009), such as ion channels (Andersson et al. 2007; Michalke et al. 2001; Steinem et al. 1997) and receptors (Goennenwein et al. 2003; Robelek et al. 2007). Consequently, a wide range of biophysical and biotechnological applications have been published, including studies of receptor-ligand interaction (Goennenwein et al. 2003), construction of screening platforms for detecting potential drug candidates (Kelety et al. 2006) as well as fabrication of biosensor (Castellana and Cremer 2006; Kim et al. 2012; Nielsen 2009) and separation (Nielsen 2009) devices.

Agnieszka Mech-Dorosz and Arto Heiskanen contributed equally to this work.

Electronic supplementary material The online version of this article (doi:10.1007/s10544-015-9936-y) contains supplementary material, which is available to authorized users.

A. Mech-Dorosz · A. Heiskanen (✉) · H. B. Muhammad · J. Emnéus
Department of Micro- and Nanotechnology, Technical University of Denmark, Produktionstorvet 423, 2800 Kgs. Lyngby, Denmark
e-mail: arto.heiskanen@nanotech.dtu.dk

S. Bäckström · M. Perry · C. Hélix-Nielsen
Aquaporin A/S, Ole Maaløes Vej 3, 2200 Copenhagen N, Denmark

S. Bäckström · C. Hélix-Nielsen
Department of Physics, Technical University of Denmark, Fysikvej 309, 2800 Kgs. Lyngby, Denmark

Published online: 04 February 2015

Many applications of biomimetic membranes and incorporated membrane proteins rely on electrochemical measurements of membrane capacitance and resistance. Free-standing black lipid membranes (BLMs), "painted" across an aperture from a lipid-containing alkane solution, based on the technique originally demonstrated by Mueller et al. (1962), are therefore still considered as the most suitable "nature-like" model for many biophysical applications on virtue of, for instance, complete access of ions and molecules to both sides of the membrane (Castellana and Cremer 2006), and formation of a defect-free lipid mosaic (Lipkowski 2010). Direct deposition of lipid bilayers on solid supports (SLBs), introduced by Tamm and McConnell (1985), has simplified the necessary experimental protocols and also resulted in electrochemical applications based on either lipid layers in direct contact with an electrode surface (Lipkowski 2010; Marquês et al. 2012; Wardak and Tien 1990) or on a self-assembled monolayer (SAM) of thiols (Michalke et al. 2001; Plant 1993; Steinem et al. 1997). However, despite successful SLB applications, these are affected by the proximity of the underlying substrate, causing differences in the lateral diffusion of lipids in the two membrane leaflets (Hetzer et al. 1998) and forming an insufficient or non-existent aqueous environment under the lipid bilayer (Castellana and Cremer 2006; Guidelli et al. 2001; Lipkowski 2010). These factors can especially hamper applications using transmembrane proteins or relying on ion transport.

A great deal of efforts have been devoted for constructing supported lipid bilayers, which are characterized by the same thermodynamic and molecular dynamic properties as free standing BLMs but without the detrimental influence of the direct substrate contact. This has been achieved creating either tethered (tBLM) or hydrated polymer (hydrogel) supported (hsBLM) lipid membranes (Knoll et al. 2008; Mccabe and Forstner 2013; Sackmann 1996; Tanaka and Sackmann 2005). In both cases, an ultrathin (often nanometer thickness) hydrophilic spacer/cushioning layer is deposited on the solid support, such as an electrode surface. The spacer of tBLMs is typically composed of hydrophilic macromolecular brushes, one end of which has a thiol functionalization facilitating formation of a SAM on the electrode surface while the other end may have a lipid moiety facilitating anchoring into the lower leaflet of the formed lipid bilayer (Knoll et al. 2008; Tanaka and Sackmann 2005). The hydrogel supports of hsBLMs are composed of a thin layer of, e.g., polyacrylamide, cellulose, agarose, polyethylene glycol, or a copolymer comprising different monomers (Mccabe and Forstner 2013; Tanaka and Sackmann 2005). Both tBLMs (Andersson et al. 2007; Knoll et al. 2008; Naumann et al. 2003) and hsBLMs (Costello et al. 1999; Kibrom et al. 2011) constructed on electrode surfaces have been applied for electrochemical recording of membrane capacitance and resistance upon introduction of ion transporters, ion channels and other membrane proteins. The decoupling between the membrane and the substrate has been demonstrated to provide an improvement for studies utilizing transmembrane proteins. However, especially in the case of tBLMs, defects and disorder in the underlying SAM (Bunjes et al. 1997; Guidelli et al. 2001) and insufficient aqueous environment in the macromolecular spacer (Leitch et al. 2009) can still influence conducted studies.

hsBLMs have emerged as the most promising way to create lipid bilayers, which approach the properties and qualities of BLMs formed across an aperture as originally demonstrated by Mueller et al (1962). Hydrogel supports do not only provide decoupling between the membrane and substrate but create a pseudo-cellular aqueous environment on both sides of the formed membrane (Kühner et al. 1994), effectively mimicking the cytosol/cytoskeleton (Kibrom et al. 2011) and extracellular matrix (Tanaka and Sackmann 2005) functionality, which ultimately facilitates design of "phantom cells" (Sackmann 1996). To enhance the aqueous environment on both sides of lipid bilayers, we have previously demonstrated the versatility of thick hydrogel supports (up to 500 μm thickness) with tunable water permeability polymerized in arrays of microapertures in ethylene tetrafluoroethylene (ETFE) partitions (Roerdink Lander et al. 2011). The combination of thick hydrogel support and microaperture arrays facilitated spontaneous thinning and stabilization of lipid membranes rapidly forming fully functional BLMs upon deposition of a lipid solution on top of the apertures without need for "painting" (manual thinning).

To further extend the versatility of our hsBLM arrays for biophysical studies and biosensor applications of BLMs, we describe in this paper a reusable device having the *in situ* polymerized hydrogel support covalently sandwiched between an electrode array microchip and the ETFE aperture array. The device interfaces the cytosol mimicking hsBLM arrays directly to electrodes for electrochemical impedance spectroscopic (EIS) measurements, which are used here together with fluorescence microscopy to characterize the stages in the device construction and the spontaneous thinning of membranes, resulting in formation of a compact lipid mosaic without defects in the continuity of lipid molecule distribution. On average, 10–15 min after introduction of a lipid solution, the formed hsBLMs reach stable membrane capacitance and resistance. The suitability and sensitivity of the device is demonstrated here using valinomycin ion transporter incorporated into hsBLMs.

2 Experimental section

2.1 Chemicals

Poly(ethylene glycol)-dimethacrylate (PEG-DMA) (PEG block, Mw. 1000 g/mol) was purchased from Polysciences,

Inc. (Warrington, PA, USA). 1,2-diphytanoyl-sn-glycero-3-phosphocholine (DPhPC) and 1-oleoyl-2-{6-[(7-nitro-2-1,3-benzoxadiazol-4-yl)amino]hexanoyl}-sn-glycero-3-phosphocholine (NBD-PC) were from Avanti Polar Lipids Inc. (Alabaster, AL, USA). 2-hydroxyethyl methacrylate (HEMA), 1,4-butanedioldiacrylate (BDDA), silicon dioxide particles (diameters 0.5–10 μm), ammonium persulfate (APS), N,N,N',N'-tetramethylethylenediamine (TEMED), 30 % hydrogen peroxide and 3-(trimethoxysilyl propyl) methacrylate (TMS-PMA), n-decane and phosphate buffered saline (pH 7.4) (PBS) were from Sigma-Aldrich Corporation (St. Louis, MO, USA). All aqueous solutions were prepared using ultrapure water (resistivity 18.2 MΩcm) from a Milli-Q® water purification system (Millipore Corporation, Billerica, MA, USA).

2.2 Fabrication and surface modification of electrode microchips

Gold electrode microchips (Fig. 1a), comprising the electrode structures (3 working electrodes (WE), one counter (CE) and one reference electrode (RE)), leads and contact pads, were fabricated according to a previously published protocol through standard lithographic process using wet-oxidized 500 μm thick 4-inch silicon wafers (one side polished) (Dimaki et al. 2014). The active electrode areas and contact pads on the patterned metal structures (10 nm Ti adhesion layer and 150 nm Au) were opened by reactive ion etching of the 500-nm thick silicon nitride layer deposited through plasma-enhanced chemical vapor deposition. The electrode microchips were cleaned for 10 min with a mixture of H_2O_2 (25 % v/v) and KOH (50 mM) followed by a potential sweep from -200 to -1200 mV in 50 mM KOH, using the on-chip three electrode set-up (Heiskanen et al. 2008). To obtain a good adhesion between the hydrogel and the electrode chip, the latter was chemically modified (Fig. 2a). To form a uniform layer of hydroxyl groups on the silicon nitride surface and gold electrodes, the chips were treated with 3 % (v/v) H_2O_2 (1 h) (Dawgul et al. 2003) and 200 mM aqueous β-mercaptoethanol (1 h), respectively. The hydroxyl groups were further functionalized by 1-h incubation in a 2 % (v/v) aqueous solution of 3-(trimethoxysilyl propyl) methacrylate at

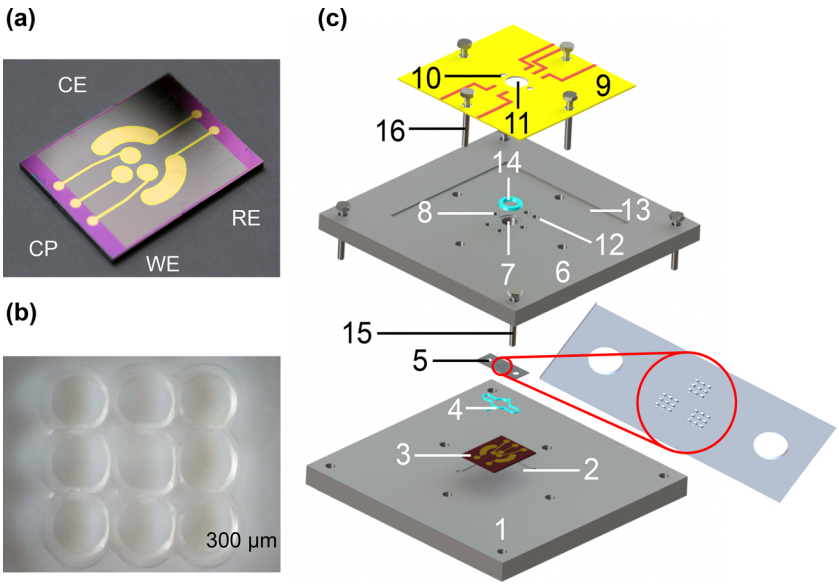

Fig. 1 **a** An image of the electrode microchip with gold electrodes: three working electrodes (WE) (active WE area: Ø 1.5 mm) surrounded by two larger electrodes used as counter (CE) and reference electrode (RE) during electrode characterization. The chip surface is passivated with silicon nitride, which is reactive ion etched to open the active electrode areas and contact pads (CP). Each electrode has a dedicated contact pad (Ø 1 mm) at the edge of the chip for electric connection to the impedance analyzer. **b** A microscope image of one 3x3 aperture array fabricated by laser ablation in the 17.2 mm×11.3 mm ETFE substrate. The diameter of each aperture is 300 μm and the distance (center-to-center) between each aperture is 400 μm. **c** A schematic view of the system assembly: 1- the bottom plate of the system assembly, 2- a recession for placement of an electrode microchip, 3- a schematic view of an electrode microchip, 4- an O-ring with a central area (Ø 5 mm) that provides access to the WEs and two "loops" (Ø 2 mm) for administering hydrogel polymerization solution, 5- an ETFE aperture array (a schematic magnification of the three 3×3 aperture arrays is shown in the insert), 6- the top plate of the system assembly, 7- a cylindrical electrochemical cell (Ø 5 mm), 8- one of the two apertures for administering hydrogel polymerization solution, 9- printed circuit board (PCB) with spring loaded pins (not visible) for electric connections, 10- one of the two openings for administering hydrogel polymerization solution, 11- an opening to the electrochemical cell, 12- one of the five apertures for electrical contacts with spring loaded pins, 13- a recession in the upper plate for placement of the PCB, 14- an O-ring for sealing the PCB around the electrochemical cell, 15- one of the four screws for assembling top and bottom plate, 16- one of the four screws for assembling the PCB to the system

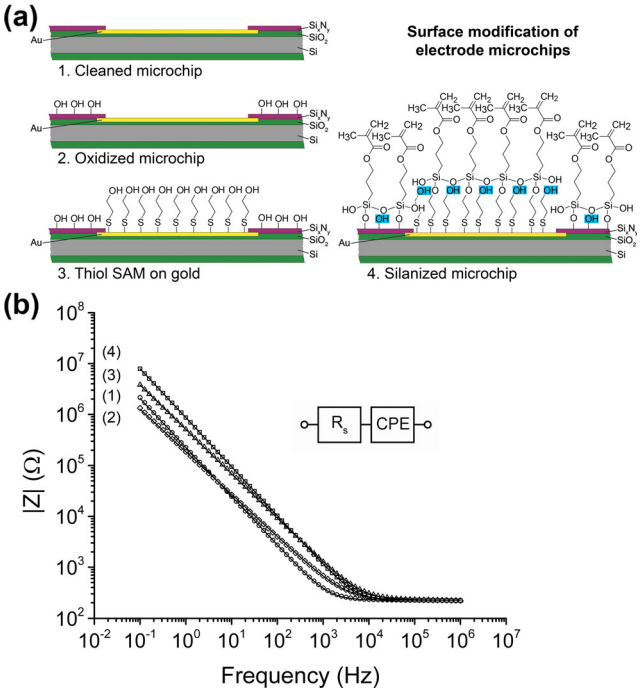

Fig. 2 **a** A schematic representation of the chemical modification of the electrode microchip to achieve a robust adhesion of the composite pHEMA hydrogel (1: a cleaned gold electrode microchip; 2: hydroxyl functionalization of the silicon nitride surface; 3: β-mercaptoethanol SAM formation on gold; 4: silanization of the microchip with TMS-PMA; the shading indicates the residual unsilanized OH-groups). **b** Representative impedance spectra acquired on one of the gold WEs on the electrode microchip after each of the modification steps shown in (a): 1: (○); 2: (◇); 3: (△); 4: (□). The *solid lines* represent NLLS fit of the data (extracted parameters shown in Table 1) to the equivalent circuit model shown in the insert (R_s – solution resistance, CPE – constant phase element). (Electrolyte: PBS – pH 7.4)

pH 4 adjusted with 1 M acetic acid (Vidič et al. 2005). After each modification step, the microchips were rinsed thoroughly with water.

2.3 Fabrication and modification of ETFE aperture arrays

The ETFE substrates (17.2×11.3 mm^2) with three 3×3-aperture (Ø=300 μm) arrays (Fig. 1b and c) were defined in Tefzel LZ200 film (thickness 50.8 μm) from DuPont Fluoropolymers (Detroit, MI, USA) using a Syndrad 48-5 S Duo Lase carbon dioxide laser (Mukilteo, WA, USA) with a power output of 50 W, as described elsewhere (Hansen et al. 2009). The fabricated aperture arrays were cleaned in acetone and ethanol followed by thorough rinsing with water. After cleaning, they were modified using a combination of water and Ar plasma in an Atto Plasma System (Diener Electronic GmbH, Ebhausen, Germany) equipped with a 13.56 MHz RF generator (3 min at the total pressure of 25 Pa and plasma power of 10 W). Immediately after plasma modification, they were subjected to either X-ray photoelectron spectroscopic (XPS) characterization and contact angle (CA) measurements or further chemical modification through silanization according to the procedure described in section 2.2. XPS characterization was done using a K-Alpha Photoelectron Spectrometer (Thermo Scientific, Waltham, MA, USA) with a nonmonochromatic AlK_α photon source (energy 1487 eV) at the anode voltage of 12 keV and pressure of 10^{-5} Pa. The energy scale was calibrated towards an Ag sample. The take-off angle of photoelectrons was 90° against the sample surface. Five areas with an elliptical shape (200-μm major radius) were analyzed on each ETFE sample. Contact angle measurements were made using an OCA 20 system (DataPhysics Instruments GmbH, Filderstadt, Germany).

2.4 Fabrication and assembly of the device components

The electrochemical measurement platform was constructed from two 6 mm thick Teflon® plates (supplied by Linatex A/S, Herlev, Denmark), depicted as the top and bottom plates (grey plates in Fig. 1c), machined using a Mini-Mill/3Pro micromilling system (Minitech Machinery Corporation, Norcross, GA, USA) executing G-code generated by EZ-CAM17 Express software (EZCAM Solutions, Inc., New York, NY, USA). The top plate defines a cylindrical electrochemical cell (height 6 mm and diameter 5 mm) and seven apertures (Ø 2 mm), two for administering hydrogel polymerization solution and five for electric contacts. The bottom plate has a recession for placement of an electrode microchip. During assembly of the platform (schematically illustrated in Fig. 1c), a tailor-made PDMS O-ring, casted in a micromilled mold using Sylgard® 184 Elastomer kit (Dow Corning Corporation, Midland, MI, USA) according to the manufacturer's standard protocol (curing at 50 °C for 12 h), was placed between the electrode array microchip and the ETFE aperture array (a magnification of a 3x3 array shown in Fig. 1b). The aperture arrays are automatically aligned on the WEs of the underlying electrode microchip by placing the ETFE aperture array in a recession in the lower side of the top plate (not shown in Fig. 1c). The construct was closed by placing the top and bottom plate against each other, and then tightened with screws. Electric contact to the underlying electrode microchip was formed using a tailor-made micromilled printed circuit board (PCB) (yellow plate in Fig. 1c) having spring loaded pins (Mill-Max Mfg. Corp., Oyster Bay, NY, USA). A tailor-made PDMS O-ring was placed between the top plate and PCB to avoid access of electrolyte under the PCB, and the system was tightened with screws.

2.5 *In situ* hydrogel polymerization

The silanized electrode microchip and ETFE aperture array in the assembled electrochemical measurement platform were further subjected to *in situ* polymerization of hydrogel. The polymerization mixture contained 23 mg PEG-DMA, 560 μl

HEMA, 8 μl TEMED, 5 μl BDDA, 140 mg silicon dioxide particles and 1000 μl MiliQ water forming a milky suspension. 60 μl of an aqueous solution of the initiator, APS (170 mg in 1000 μl MiliQ water), was added immediately prior to polymerization. The mixture was vortexed for 10 s and introduced immediately through the filling aperture of the top plate (Fig. 1c). The excess of the polymerization solution was allowed to flow out through the aperture on the opposite side. After polymerization, the pHEMA was hydrated by filling the well of the electrochemical cell with PBS and stored for 24 h at room temperature. A schematic view of the hydrogel "sandwiched" between the ETFE partition array and gold electrode microchip can be seen in Fig. 3.

2.6 BLM formation

The lipid solution for BLM formation contained 495 μl of DPhPC stock solution (25 mg/ml) doped with 24 μl of NBD-PC stock solution (1 mol%), a fluorescence probe used for fluorescence microscopic analysis of lipid membranes. Commercially available DPhPC and NBD-PC lipid solutions in chloroform (10 mg/ml) were dried under nitrogen gas flow and subsequently redissolved in decane. The lipid solution was prepared 1 day before use and stored at -20 °C until use. Prior to the electrochemical measurements, the ETFE array was pretreated according to previously described procedure by applying 4 μl of lipid solution in decane, which was allowed to evaporate for 10 min at room temperature (Roerdink Lander et al. 2011). After that, the electrochemical cell was filled with 100 μl of PBS followed by filling the apertures of the three 3×3 ETFE arrays with 4 μl of the lipid solution.

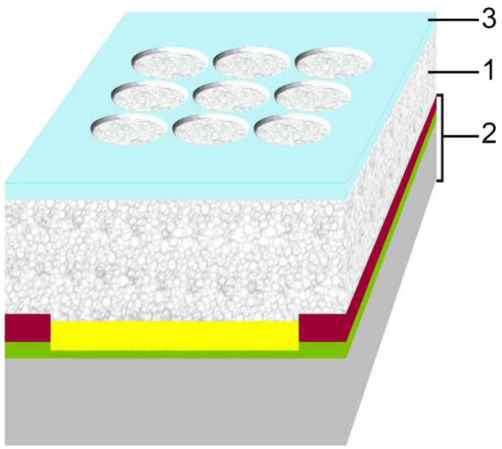

Fig. 3 A schematic representation of the covalent "sandwich" structure suitable as lipid membrane support: (1) The composite pHEMA hydrogel is covalently sandwiched between (2) the silanized electrode microchip (*grey* - silicon wafer; *green* – silicon oxide, *yellow* – cross section of a gold electrode, *red* – silicon nitride) and (3) ETFE aperture array

2.7 Incorporation of valinomycin in BLMs

Valinomycin stock solution (1.8 mM in 96 % ethanol) was stored at 4 °C until use in experiments. BLMs were formed as described in section 2.6. After BLM formation, the concentration of K^+ was elevated from the original 2.7 mM in PBS to 20 mM while retaining the total volume at 100 μl. After having acquired an impedance spectrum at the elevated K^+ concentration in the presence of the formed BLMs, 2 μl of the valinomycin stock solution was added in the vicinity of the BLMs, corresponding to 35 μM (Hansen et al. 2009) in the total volume. An impedance spectrum was acquired immediately after addition of valinomycin and repeated twice at 5 min interval.

2.8 Fluorescence microscopic visualization of BLMs

Fluorescence imaging of BLMs using the fluorescent probe NBD-PC was performed under a Zeiss Axio Imager M1m microscope equipped with an AxioCam MRc5 computer controlled CCD camera, 2.5x objective and filter set 38 (Carl Zeiss AG, Göttingen, Germany). The images were acquired using Zeiss AxioVision software (V. 4.8).

2.9 Electrochemical characterization

Each step of electrode microchip modification was characterized (see Fig. S1 in the Electronic supplementary material for the electrochemical cell used for characterization of electrode modifications) by electrochemical impedance spectroscopy (EIS) using the on-chip CE and RE (frequency range: 100 mHz – 1 MHz; 10 data points per decade). The capacitive and resistive properties of the ETFE/hydrogel support, covalently attached on the electrode array microchip, and the formed BLMs were characterized by EIS using a platinum wire CE placed at a distance of 1.5 mm (height adjustment using a micromanipulator) from the top of the ETFE aperture array (frequency range: 1 Hz – 1 MHz; 5 data points per decade). In each case, the applied sinusoidal potential had the amplitude of 10 mV_{rms} with respect to the open circuit potential. EIS analysis was performed using a computer controlled Reference 600 potentiostat from Gamry Instruments (Warminster, PA) operated by EIS300 software (V. 5.30). Data analysis was done using EchemAnalyst software (V. 6.10) from Gamry Instruments by fitting the data to equivalent circuit models using nonlinear least-squares (NLLS) regression.

3 Results and discussion

Applications of, e.g., ion channels, ligand-receptor interaction and GPCR activation, require stable lipid membranes

associated with an aqueous environment to facilitate membrane protein reconstitution under conditions resembling their native state in living cells. In our previous study, we demonstrated formation of hydrogel supported black lipid membranes (hsBLMs) across an ETFE aperture array. The hydrogel was initially formed in a mold and transferred to the measurement platform to function as a partition between the cis and trans chamber (Roerdink Lander et al. 2011). In comparison with free-standing BLMs suspended only in an ETFE aperture array (Hansen et al. 2009), the hydrogel supported lipid membranes were characterized by a prolonged lifetime and spontaneous self-thinning process resulting in BLM formation.

In the present study, we address the design, fabrication and characterization of a compact analysis device aimed for studies on hsBLMs, demonstrating the versatility of integrating an electrode microchip with an *in situ* polymerized hydrogel support connected to an ETFE aperture array. Hence, only one chamber is required for depositing a lipid solution and conducting EIS measurements on arrays of hsBLMs associated with a pseudo-cellular matrix. Once assembled, the platform facilitates continuous usage in experiments. Both the *in situ* polymerized hydrogel support and hsBLMs are formed simultaneously on each working electrode, improving reproducibility and facilitating parallelization of measurements. The presented device concept serves as a basis for further development of miniaturized devices (Zagnoni 2012) for automated experiments on hsBLMs under fluidic control.

3.1 Construction and characterization of ETFE/hydrogel support on gold electrode microchips

For successful function of a hydrogel support interfaced with an electrode microchip and ETFE aperture array, i) there should be no electrolyte flux around the hydrogel to the electrode surface, and ii) the hydrogel should have a strong contact with the ETFE substrate for effective stabilization of the formed BLMs. Preliminary experiments indicated that only by achieving a sufficient adhesion of the *in situ* polymerized hydrogel on the electrode microchip and the ETFE substrate both requirements could be met. To achieve this goal, covalent sandwiching of the *in situ* polymerized hydrogel between the gold electrode microchip and the ETFE aperture array (schematically illustrated in Fig. 3) was performed. The electrode microchip-hydrogel-ETFE construct is encased in the Teflon® housing schematically shown in Fig. 1c. A detailed description and characterization of all the steps of electrode microchip and ETFE aperture array modification leading to the covalently sandwiched hydrogel are presented below.

3.1.1 Modification and characterization of gold electrode microchips

The electrode microchips (Fig. 1a), comprising three working electrodes (WE) surrounded by two larger electrodes (counter and reference electrode during electrochemical characterization of electrode modifications), were fabricated using standard UV-lithography. The active electrode areas were defined in the insulating silicon nitride layer using reactive ion etching. To provide covalent bonding of the hydrogel (primarily composed of 2-hydroxyethyl methacrylate monomers), both material constituents of the electrode microchips, i.e. gold and silicon nitride, needed to be modified with acrylate functionalities to allow participation during *in situ* polymerization. To achieve acrylate functionalization in a one-step modification reaction, both silicon nitride and gold surfaces had to be converted initially to intermediary hydroxyl functionalities.

A thin oxide layer can be formed on silicon nitride surfaces during storage at ambient condition. However, initial functionalization tests of silicon nitride surfaces having the native oxide layer present (or after removing it (Sung et al. 1999)) using silane coupling agents (Ulman 1996) were not successful. The polymerized hydrogel was readily detached from the microchip surface. Tests with H_2O_2 oxidation of silicon nitride (Dawgul et al. 2003) proved to form a sufficiently dense hydroxyl functionalization, which after silanization with TMS-PMA followed by hydrogel polymerization yielded a hydrogel that could not be removed from the silicon nitride surface without breaking the bulk polymer and leaving a residual layer.

Functionalization using alkane thiols with different end groups is well established for modification of metal surfaces (Ulman 1996). Hence, β-mercaptoethanol SAM can be used to obtain a coverage of hydroxyl functionalities on gold, facilitating silanization with TMS-PMA, which is analogous to silanization of β-mercaptoethanol modified quantum dots using amino functionalized silane (Wu et al. 2011). Modification tests of gold surfaces followed by hydrogel polymerization yielded a strongly bonded hydrogel similarly as for the modified silicon nitride surfaces. A schematic view of all the modification steps adapted for silicon nitride/gold surfaces is shown in Fig. 2a.

The chemical modifications of the electrode microchips were characterized using EIS, which has been widely applied for characterization of electrode modifications in biotechnological applications (Guan et al. 2004; Heiskanen et al. 2008). EIS-based characterization of the electrode interface after chemical modifications allows comparison with the interface in the presence of hydrogel and BLMs. Figure 2b shows typical impedance spectra (impedance magnitude vs. frequency on a logarithmic scale) of a bare gold electrode and the same electrode after sequential modification steps (hydroxylation of silicon nitride surface, β-mercaptoethanol SAM formation on

gold and silanization). The spectra were fitted to the equivalent circuit model shown in the insert of Fig. 2b, which represents the ohmic resistance of an electrolyte (R_s) (may also comprise the impedance of electric connections to an impedance analyzer) in series with the double layer capacitance of the electrode surface. The purely capacitive behavior of the double layer has been replaced by the impedance of a constant phase element (CPE), which more accurately represents a solid electrode interface showing current distribution due to surface inhomogeneity (Brug et al. 1984).

The CPE parameters, Q representing the magnitude of CPE and α, which is a constant having a value between 0 and 1, obtained from the NLLS fit of the spectra to the equivalent circuit model, were converted to an effective equivalent capacitance (C_{eff}) to provide an easier comparison. Since the presented impedance spectra (Fig. 2b) were acquired in PBS without any faradaic processes taking place, the conditions resemble those of a blocking electrode (Brug et al. 1984; Hirschorn et al. 2010), for which $C_{eff}=[QR_e^{(1-\alpha)}]^{1/\alpha}$, where R_e, the global ohmic resistance of the system when the angular frequency $\omega\rightarrow\infty$, may be approximated by R_s. Table 1 shows the values of R_s, Q and α together with the corresponding value of C_{eff} after each electrode treatment. The applied gold cleaning procedure generates a reduced gold surface (Heiskanen et al. 2008), the double layer capacitance of which is decreased by each modification step in accordance with the general behavior of electrode modifications as capacitors in series with the double layer capacitance of a bare metal electrode (Heiskanen et al. 2008). The values of α, being about 0.960, indicate that the electrode interface behavior is close to a pure capacitance. However, after H_2O_2 treatment, the resulting oxidized gold surfaces show a significant decrease in α indicating an increased inhomogeneity of the interface, which is, though, eliminated by thiol SAM formation.

3.1.2 Modification and characterization of ETFE aperture arrays

In an analogous manner, as was presented above for the electrode microchip modification, incorporation of covalently bound acrylate functionalities on ETFE can result in covalent tethering of the *in situ* polymerized hydrogel. ETFE, a copolymer composed of alternating CH_2-CH_2 and CF_2-CF_2 units, is chemically inert and highly hydrophobic. Plasma modification of fluorohydrocarbons, such as ETFE, has been demonstrated as an effective means to achieve surface functionalization. Especially, Ar plasma has been shown to increase the oxygen contents on ETFE surfaces, however, primarily by carbonyl functionalization (Inagaki et al. 2002). Modification of ETFE substrate using Ar plasma in the presence of HEMA monomers has been reported to covalently bond to an ETFE substrate facilitating tethering of an *in situ* polymerized pHEMA hydrogel (Roerdink Lander et al. 2011). Preliminary results in the present study indicated, however, that for sandwiching of the hydrogel support between an electrode microchip and ETFE substrate, such a modification was not sufficiently robust.

To obtain a modification of the ETFE aperture array analogous to that of the electrode microchip (sections 2.2 and 3.1.1), the combination of Ar and H_2O plasma was optimized.

Table 1 Extracted EIS parameter values for characterization of electrode modifications, ETFE/hydrogel construct, and BLM formation on one working electrode (WE)

Electrode microchip preparation	Q [nS s^{α}]	α	C_{eff} [nF]	$R_{ser,hg}$ [Ω]	$R_{par,hg}$ [Ω]	$C_{par,hg}$ [pF]	R_m [Ω]	C_m [nF]
Cleaning[b]	758	0.960	528[f]	n/a	n/a	n/a	n/a	n/a
Hydroxylation[b,c]	1161	0.835	227[f]	n/a	n/a	n/a	n/a	n/a
Thiol SAM[b]	230	0.961	156[f]	n/a	n/a	n/a	n/a	n/a
Silanization[b]	198	0.963	134[f]	n/a	n/a	n/a	n/a	n/a
ETFE/hydrogel[d]	320	0.934	180[g]	745	1.8×10^3	530	n/a	n/a
BLM array on hydrogel support[e]	8.2	0.98	n/a	2.4×10^3	8.5×10^6	22	10.1×10^6	1.9

Calculated value of effective equivalent capacitance (C_{eff}) based on the parameters (Q and α) of constant phase element impedance (Z_{CPE}) for each electrode microchip treatment

n/a – not applicable

[a] Uncertainty between individual WEs±8 %

[b] Impedance spectra and equivalent circuit model in Fig. 2b

[c] Silicon nitride hydroxylation with H_2O_2 leads to electrode oxidation

[d] Impedance spectrum and equivalent circuit model in Fig. 5

[e] Impedance spectrum and equivalent circuit model in Fig. 6c

[f] In the conversion of Z_{CPE} to C_{eff}, $R_e\equiv R_s$ was 225 Ω

[g] In the conversion of Z_{CPE} to C_{eff}, $R_e\equiv R_s+R_{ser,hg}$ was 970 Ω

H_2O plasma can generate hydroxyl functionalities on polymer surfaces already containing, for instance, carbonyl functionalities (Long et al. 2006; Tompkins et al. 2013), facilitating silanization (Long et al. 2006). To minimize surface etching of ETFE, easily caused by Ar plasma primarily composed of ions (Inagaki et al. 2002), the plasma generation power was set to 10 W and the exposure time was set to 3 min. In the utilized plasma system, Ar and H_2O were introduced simultaneously through separate inlets under the total pressure of 25 Pa. In previous studies using H_2O plasma, a significantly higher power has been applied (Long et al. 2006; Tompkins et al. 2013). However, in this study, the decreased power and longer exposure time were sufficient for the functionality-introducing surface reactions of the radical species (e.g., OH·and H·) characteristic of H_2O plasma (Steen et al. 2001). Silanization of the plasma modified ETFE substrates with TMS-PMA yielded a sufficiently dense acrylate functionalization, resulting in strongly bonded hydrogel, which in peeling tests left hydrogel residues on the modified ETFE surfaces. Although only a brief optimization of the plasma conditions was conducted, the results can guide further optimization (e.g., serial introduction of Ar and H_2O under different power, pressure and exposure time). To our best knowledge, this study presents the first demonstration of the applicability of Ar/H_2O plasma for modification of ETFE surfaces with subsequent silanization.

Three different sets of ETFE samples (untreated, Ar plasma treated and Ar/H_2O plasma treated) were characterized using both XPS and water CA measurements. Typical XPS spectra of C_{1s} and O_{1s} for untreated and plasma treated ETFE surfaces are shown in Fig. 4a and b, respectively. The averaged oxygen/carbon (O/C) ratio, binding energies (BE) together with the assigned chemical components (based on XPS characterization), and CA values are summarized in Table 2. Untreated samples of ETFE showed the presence of oxygen, which is assigned to adsorbed oxygen (Samide et al. 2010) during storage of ETFE sheets. The two observed carbon peaks at 290.9 eV and 286.0 eV represent CF_2 and CH_2 components, respectively (Inagaki et al. 2002). Under the applied plasma conditions, an increase in O/C ratio was observed, being most prominent when using the combination of Ar/H_2O plasma. Based on the shift in both carbon and oxygen binding energy to slightly higher values, the effect of Ar plasma was attributed to an increased carbonyl (C=O) functionalization (Inagaki et al. 2002), while the effect of Ar/H_2O plasma was attributed to the combination of C=O and hydroxyl (OH) (Samide et al. 2010) functionalization. No significant shift was observed in the carbon peak corresponding to CF_2. Moreover, the fluorine/carbon ratio remained unchanged (results not shown). Together these findings indicate that under the applied plasma conditions neither Ar nor Ar/H_2O plasma caused defluorination of ETFE unlike was shown by Inagaki et al. (2002), the modifications being limited to the ethylene components of ETFE. The CA decreased significantly as a consequence of both Ar and Ar/H_2O plasma treatment, corroborating the observed increase in oxygen contents.

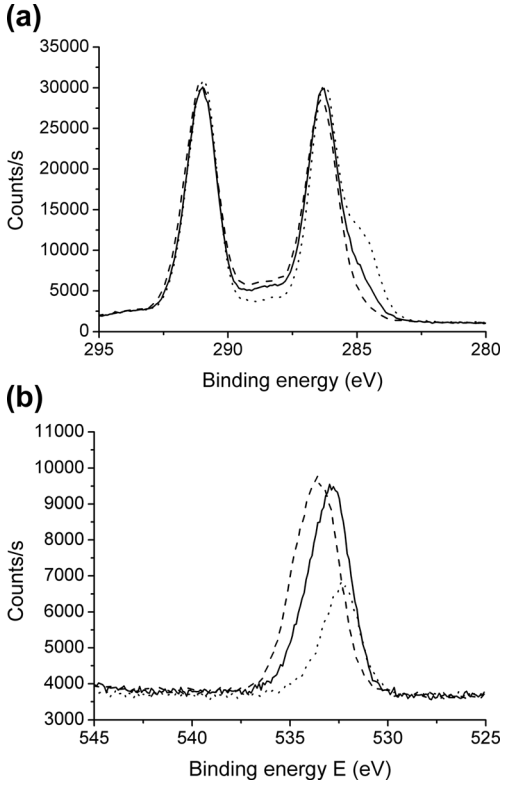

Fig. 4 Typical (**a**) C_{1s} and (**b**) O_{1s} XPS spectra of ETFE surfaces: Untreated ETFE ( ), Ar plasma treated ETFE (——), and Ar/H2O plasma treated ETFE (- - -)

3.1.3 EIS characterization of ETFE/hydrogel support

The assembly of the device (Fig. 1c) resulted in a 500 μm high fluidic path between the electrode microchip and ETFE aperture array, facilitating introduction of silane solution followed by the hydrogel polymerization solution. During the silanization step, both the electrode microchip and ETFE substrate were modified with methacrylate moieties, which were then incorporated into the formed hydrogel, facilitating covalent sandwiching. The constructed ETFE/hydrogel support integrated on the electrode microchip was characterized using EIS measurements to provide a deeper understanding of its capacitive and resistive properties as a prerequisite for the study of hsBLMs.

Figure 5 shows a characteristic impedance spectrum of a hydrogel covalently sandwiched between an ETFE aperture array and electrode microchip. To provide a reference for comparison, the impedance spectrum obtained after silanization of the electrode microchip is included in the figure (dashed line). Significant differences in the impedimetric behavior can be observed throughout a wide frequency range

Table 2 XPS analysis of oxygen/carbon molar ratio (O/C), C_{1s} and O_{1s} binding energy (BE) with assignment of the corresponding chemical components, and measured water contact angle (CA) of untreated, Ar plasma and Ar/H2O plasma treated ETFE substrates

ETFE sample treatment (plasma)	XPS							CA
	O/C (%mol)	C_{1s} (peak 1)		C_{1s} (peak 2)		O_{1s}		
		BE (eV)	Chemical component	BE (eV)	Chemical component	BE (eV)	Chemical component	(°)
Untreated	0.02	286.0	CH_2	290.9	CF_2	532.4	$O_{adsorbed}$	103
Ar	0.06	286.2	C=O	291.0	CF_2	533.0	C=O	88.7
Ar/H_2O	0.08	286.4	CH_2-OH	291.0	CF_2	534.0	CH_2-OH	78.4

(from ~100 Hz to 1 MHz). Hence, to fit the spectrum, the equivalent circuit representing a cleaned/chemically treated gold electrode (Fig. 2b) was modified, including an additional resistor in series ($R_{ser,hg}$) with solution resistance (R_s) and an additional time constant in the form of a capacitor ($C_{par,hg}$) and resistor ($R_{par,hg}$) in parallel (Fig. 5). The analysis of the spectrum in Fig. 5 (summarized in Table 1) shows that the presence of the hydrogel causes an increased resistance to ionic current ($R_{ser,hg}$). The covalent bonding of the hydrogel makes it an integral part of the electrode interface impedance, significantly changing the parameters of the Z_{CPE} from the ones obtained after silanization. The decrease in α indicates a decrease in the surface homogeneity. A calculation shows that the observed change in Z_{CPE} corresponds to an increase in the charge storing capacity of the electrode interface (C_{eff}). Due to the thickness of the hydrogel (500 μm), its bulk structure also

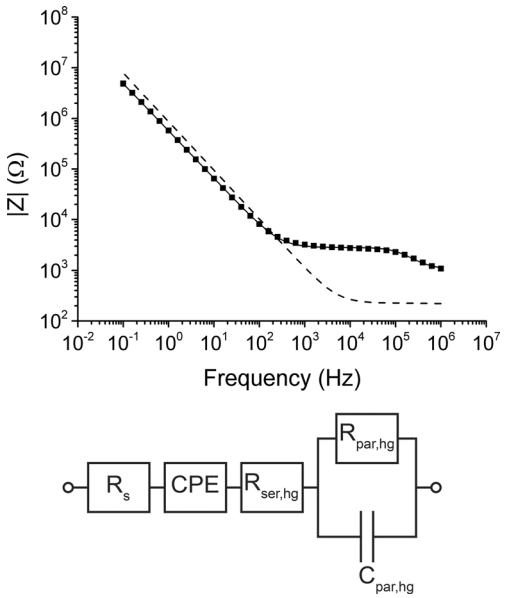

Fig. 5 An impedance spectrum (■) acquired on the chemically modified WE (Fig. 2) after covalent attachment of ETFE/hydrogel support on the microchip. The *solid line* represents the NLLS fit of the data (extracted parameters in Table 1) to the equivalent circuit model shown in the insert ($R_{ser,hg}$ – ETFE/hydrogel resistance in series, $R_{par,hg}$ – ETFE/hydrogel resistance in parallel, $C_{par,hg}$ – ETFE/hydrogel capacitance in parallel). The *dashed line* represents the impedance spectrum acquired on the same WE after silanization (Fig. 2b)

constitutes a capacitive ($C_{par,hg}$) and resistive ($R_{par,hg}$) pathway, indicating more complex impedance properties compared to nanometer hydrogels (Kibrom et al. 2011).

3.2 Characterization of hsBLMs

3.2.1 Fluorescence microscopic visualization of membrane formation

Upon depositing the lipid containing decane solution on top of the ETFE aperture arrays, a multilayer of lipids fill the apertures and partially cover the surrounding surface of the ETFE substrate, which in the presence of the fluorescent probe (NBD-PC) appear intensely green (Fig. 6a; left panel). The hydrogel support induces a spontaneous spreading of the solvent towards the edges of the apertures resulting in thinning of the lipid layer inside the apertures. During continuous microscopic observation, the progress of the thinning is seen as the fluorescing area in each apertures diminishes when the membrane reaches the thickness of a few nanometers characteristic of a lipid bilayer (Ries et al. 2004). Further expansion of the black lipid bilayer area leaves only a fluorescing solvent filled annulus (Fig. 6a (right panel) and schematically shown in Fig. 6b). The remaining annulus in each aperture serves as a stabilizing bridge between the thinned membrane and the edge of the aperture. The dimension of the annuli in the entire aperture array determines the total area occupied by the formed membrane, which based on a rough estimation is on average 80–90 % of the total area of the apertures.

3.2.2 Membrane array characterization using EIS

Traditionally, monitoring of the capacitance and resistance of a membrane formed either across a single aperture or an array of apertures is conducted through voltage clamp measurements by placing an electrode on each side of the membrane (Roerdink Lander et al. 2011). For data analysis, a parallel circuit of a resistor and capacitor is a suitable model describing the membrane resistance and capacitance, respectively. Even in a system utilizing a hydrogel support together with an aperture array, a parallel circuit is a sufficiently good

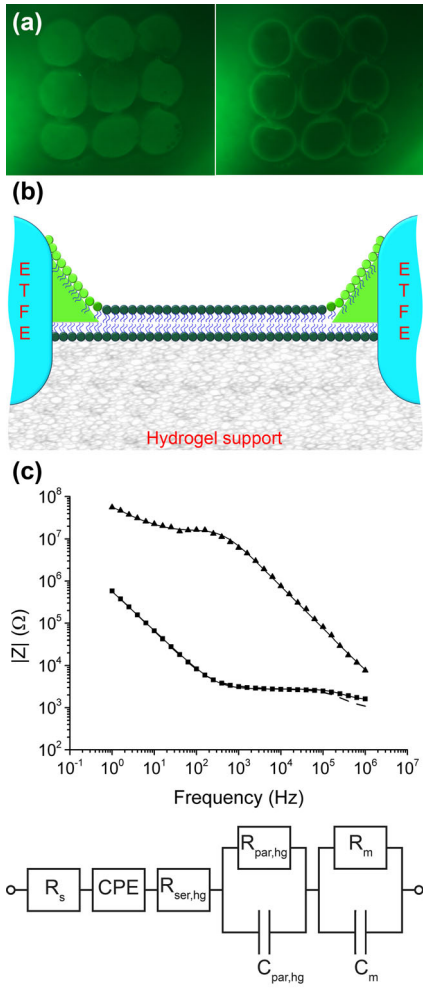

Fig. 6 **a** Fluorescence microscopic visualization of lipid membrane formation: (Left panel) Distribution of the lipid solution immediately after introduction on the ETFE substrate. A thick fluorescing lipid layer covers the ETFE surface filling the apertures. (Right panel) Progress of BLM formation (spontaneous thinning of the lipid layer) initiated by spreading of the solvent towards the edges of the apertures in the ETFE substrate (the image was acquired 4 min after introduction of the lipid solution). **b** A schematic view of a hydrogel supported hsBLM formed in an aperture. The formed solvent annulus is shown in the periphery of the aperture. **c** An impedance spectrum (▲) acquired on the WE with the covalently attached ETFE/hydrogel support (Fig. 5) after formation of hsBLMs (15 min after introduction of the lipid solution). The solid line represents the NLLS fit of the data (extracted parameters in Table 1) to the equivalent circuit model shown in the insert (C_m – membrane capacitance, R_m – membrane resistance of the BLM array). An impedance spectrum (■) acquired on the same WE after disruption of the BLMs. The solid line represents the NLLS fit of the data to the equivalent circuit model shown in Fig. 5. The dashed line represents the impedance spectrum acquired on the same WE after covalent attachment of the ETFE/hydrogel support (Fig. 5). (Electrolyte: PBS – pH 7.4)

approximation of the properties of the membrane since the impedance of the hydrogel can be considered negligible in comparison with that of the membrane (Roerdink Lander et al. 2011). In EIS measurements, commonly used to study lipid bilayers on an electrode surface (Knoll et al. 2008; Michalke et al. 2001; Naumann et al. 2003; Plant 1993; Steinem et al. 1997), the interface impedance of the underlying electrode has to be taken into consideration when analyzing the measurement data. The equivalent circuit describing the acquired impedance spectra comprises solution resistance in series with the double layer capacitance combined with a parallel circuit of the membrane resistance and capacitance (Knoll et al. 2008; Michalke et al. 2001; Naumann et al. 2003; Steinem et al. 1997). When a hydrogel support is covalently tethered on the underlying electrode, as is the case in the device presented here, the total impedance comprises both the electrode surface and the bulk hydrogel (Fig. 5).

Figure 6c shows a typical impedance spectrum for hsBLMs formed in the 3x3 ETFE aperture array. For comparison, the impedance spectrum acquired after *in situ* polymerization of the hydrogel has been included in the figure (dashed line). Figure 6c shows the equivalent circuit model that includes the influence of the hydrogel combined with a parallel circuit accounting for the membrane capacitance (C_m) and resistance (R_m). NLLS analysis of the spectrum yields C_m and R_m for the entire 3x3 array of hsBLMs (Table 1). The array specific membrane capacitance ($C_{m,sp}$) can be obtained by normalization of C_m with respect to the area occupied by hsBLMs. As shown in Fig. 6a (right panel) and b, due to the formed solvent annulus, the total area of hsBLMs is smaller than the area determined by the diameter of the apertures (0.00636 cm^2). If considering an average area of hsBLMs equal to 85 % of the total area of the apertures, the calculated $C_{m,sp}$ for the hsBLMs represented by the spectrum in Fig. 6c is 0.35 $\mu F/cm^2$, which is in the same range as we previously showed for hsBLMs formed in 8x8 ETFE aperture arrays (Roerdink Lander et al. 2011). Based on a corresponding estimation, the array specific membrane resistance ($R_{m,sp}$) is over 54 $k\Omega\ cm^2$.

EIS characterization of the hsBLM arrays indicated that the stabilized $C_{m,sp}$ varied from experiment to experiment in the range from 0.31 to 0.49 $\mu F/cm^2$. Correspondingly, the $R_{m,sp}$ varied between 45 and 65 $k\Omega\ cm^2$. Benz et al. have reported 0.3–0.4 $\mu F/cm^2$ as the characteristic range of specific membrane capacitances for decane-containing free-standing BLMs (Benz et al. 1975), which indicates that the formed hsBLMs are primarily decane containing. The presence of the hsBLMs also causes changes in $C_{par,hg}$ (range: 20–30 pF) and $R_{par,hg}$ (range: 5–10 MΩ), as well as the double layer capacitance (represented by Z_{CPE}: Q in the range of 8–10 nS s^{α} and $\alpha \rightarrow 1$) from the values characteristic of the hydrogel without BLMs (Table 1). This leads to the conclusion that the hydrophilic side of the lower leaflet of the lipid membrane is directly interacting with the hydrogel support as illustrated in Fig. 6b.

Due to spontaneous thinning of the deposited lipid solution, resulting in BLM formation promoted by the hydrogel support, the stabilized $C_{m,sp}$ and $R_{m,sp}$ could be obtained in roughly 10 min (details of the spontaneous thinning of membranes monitored as a function of time using voltage clamp are shown in Fig. S2 in the Electronic supplementary

material). Considering this time window, experiments on hsBLMs could be conducted under stable conditions 15 min after deposition of the lipid solution. After stabilization of $C_{m,sp}$ and $R_{m,sp}$, the life time of hsBLMs varied between 60 and 80 min, which is similar to our previous study where the hydrogel support was formed during *ex situ* polymerization (Roerdink Lander et al. 2011). If the thinning process is not completed, the acquired impedance spectra show discrete steps due to changes in the lipid layer thickness that are faster than the acquisition time of a spectrum (an example is shown in Fig. S3 in the Electronic supplementary material). NLLS analysis of such spectra does not yield very accurate estimations of C_m and R_m although rough estimations show that immediately after deposition of the lipid solution, the values are below 100 pF and 30–40 MΩ, respectively, indicating the presence of a thick lipid layer.

Occasionally, sudden discrete changes were observed in the acquired impedance spectra of the initially stabilized hsBLMs, which were interpreted as further thinning due to elimination of solvent from the annuli. In such cases, the estimated $C_{m,sp}$ rose above 0.6 μF/cm^2 (details of the further membrane thinning monitored as a function of time using voltage clamp are shown in Fig. S2 in the Electronic supplementary material). However, removal of solvent from annuli compromises the stability of hsBLMs and their remaining lifetime is shortened. When under such conditions all the individual hsBLMs in an array are broken, the resulting impedance spectrum shows essentially the baseline behavior of the original hydrogel ($C_{par,hg}$, $R_{par,hg}$, and Z_{CPE} return to values prior to hsBLM formation) with only a slight increase in the high-frequency impedance reflected by the value of $R_{ser,hg}$. A typical impedance spectrum acquired after hsBLMs were broken is shown in Fig. 6c, indicating a complete overlap with the spectrum of the hydrogel before hsBLM formation in the frequency range below 100 kHz. This behavior can be explained by the fact that both the solvent and lipids are removed from the apertures due to phase separation in the aqueous medium.

3.2.3 EIS characterization of valinomycin incorporation into hsBLM array

Incorporation of the potassium ion transporter valinomycin was used to characterize the sensitivity of the constructed platform in monitoring changes in C_m and R_m. Figure 7 shows a set of typical impedance spectra acquired in the presence of 20 mM K^+ before and after incorporation of valinomycin in an hsBLM array. The insert shows a magnified view of the spectra in the frequency range between 1 Hz and 1 kHz where the influence of valinomycin is most clearly manifested. The spectra were analyzed using the equivalent circuit model in Fig. 6c. It can serve as an approximation of the effect of valinomycin-mediated K^+ transport (Naumann et al. 2003), which does not require the presence of a diffusion impedance

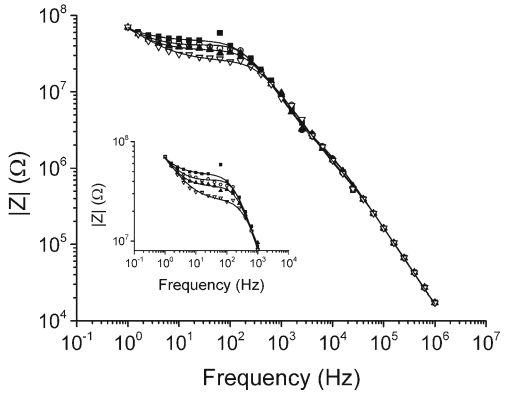

Fig. 7 An impedance spectrum (■) acquired on the WE with the covalently attached ETFE/hydrogel support (Fig. 5) after formation of BLMs (15 min after introduction of the lipid solution); impedance spectra acquired immediately (t=0) (○), 5 min (▲), and 10 min (▽) after introduction of valinomycin. The *solid lines* represent NLLS fit of the data (calculated values of $R_{m,sp}$ and $C_{m,sp}$ in Table 3) to the equivalent circuit model shown in Fig. 6c. The insert shows a magnified view of the spectra in the frequency range from 1 Hz to 1 kHz. (Electrolyte: PBS – pH 7.4, [K^+]=20 mM; [Valinomycin]=35 μM)

characteristic of ion channels (Michalke et al. 2001; Steinem et al. 1997). Although the total concentration of K^+ (20 mM) in the solution was only 1/10 of the one used in our previous study (Hansen et al. 2009), demonstrating the function of valinomycin in hsBLMs in an ETFE aperture array, the observed trend in membrane resistance is the same. During the first 5 min after introduction of valinomycin, only a gradual decrease in R_m could be seen, whereas after 10 min the maximal decrease was obtained. Correspondingly, C_m increased with time although the changes were not drastic, which is in accordance with results reported elsewhere for solid supported lipid membranes with incorporated valinomycin (Naumann et al. 2003). Table 3 shows the calculated values of $C_{m,sp}$ and $R_{m,sp}$ based on the same assumption of the effective hsBLM area as described in section 3.2.2. The presented validation of the functionality of the device using valinomycin, as well as incorporation of α-hemolysin in our previous study

Table 3 Calculated array specific membrane capacitance ($C_{m,sp}$) and resistance ($R_{m,sp}$) before and after introduction of valinomycin

Experimental condition[a]	$C_{m,sp}$[c,d] [μF/cm^2]	$R_{m,sp}$[c,d] [kΩ cm^2]
No valinomycin	0.35	58
Valinomycin[b] (t=0)	0.37	48
Valinomycin[b] (t=5 min)	0.40	44
Valinomycin[b] (t=10 min)	0.42	32

[a] Electrolyte: PBS (pH 7.4), [K^+]=20 mM

[b] [Valinomycin]=35 μM

[c] Calculated based on spectra in Fig. 7

[d] Data fitted to the equivalent circuit model in Fig. 6c

(Roerdink Lander et al. 2011), outline the potential of the device for lipid membrane studies. Upon further validation using functional proteins and other mobile ion transporters the scope of applications can be extended.

4 Conclusion

We fabricated a reusable device for electrochemical impedance spectroscopic (EIS) monitoring of hydrogel supported black lipid membranes (hsBLMs) formed in an ethylene tetrafluoroethylene (ETFE) aperture array. The novel feature of the device is the *in situ* polymerized hydrogel, primarily composed of poly(2-hydroxyethyl methacrylate) (pHEMA), covalently sandwiched between a silicon-based gold electrode microchip with three working electrodes and an ETFE aperture array both functionalized using 3-(trimethoxysilyl propyl) methacrylate. To allow silanization, the surfaces of the material constituents of the electrode microchips, gold and silicon nitride, were hydroxylated by β-mercaptoethanol SAM and hydrogen peroxide oxidation, respectively. Correspondingly, hydroxylation of ETFE surfaces was achieved using an optimized Ar/H_2O plasma treatment. The modification steps of the electrode microchips and polymerized hydrogel were characterized using EIS, and the plasma modification of ETFE was characterized using the combination of XPS and contact angle measurements. Conducted fluorescence microscopic and EIS monitoring of hsBLMs demonstrated the versatility of the device in facilitating spontaneous thinning of membranes without need for manual painting, reaching stabilization of membrane capacitance and resistance in about 10 min. The functionality of the device and sensitivity of the integrated electrodes in EIS detection were demonstrated by incorporation of valinomycin in hsBLMs. Further work is being conducted to demonstrate the potential of the device for studies involving functional proteins and other mobile ion transporters. This work also comprises further improvement of membrane life time by optimization of aperture size/number per electrode, precision of aperture patterning to enhance the stability of the formed annuli, and smoothening of the hydrogel support using layer-by-layer deposited polyelectrolytes. Although the electrochemical cell of the assembled platform is reusable and facilitates continued experimentation on three electrodes, parallelization of the platform can be increased by redesigning electrode microchips. Furthermore, the construct of sandwiched hydrogel can be incorporated in a microfluidic environment for automated experiments on hsBLMs.

Acknowledgments This work was financially supported by the Copenhagen Research School of Nanotechnology (CONT) from Denmark, Department of Micro- and Nanotechnology at Technical University of Denmark and a cleantech company Aquaporin A/S in Copenhagen, Denmark. Additionally, A. H. acknowledges Lundbeck Foundation grant no. R69-A6408 for financial support.

References

M. Andersson, H.M. Keizer, C. Zhu, D. Fine, A. Dodabalapur, R.S. Duran, Langmuir **23**, 2924 (2007)
R. Benz, O. Frölich, P. Läuger, M. Montal, Biochim. Biophys. Acta **394**, 323 (1975)
G.J. Brug, A.L.G. van den Eeden, M. Sluyters-Rehbach, J.H. Sluyters, J. Electroanal. Chem. **176**, 275 (1984)
N. Bunjes, E.K. Schmidt, A. Jonczyk, F. Rippmann, D. Beyer, H. Ringsdorf, P. Gra, W. Knoll, R. Naumann, Langmuir **13**, 6188 (1997)
E.T. Castellana, P.S. Cremer, Surf. Sci. Rep. **61**, 429 (2006)
R.F. Costello, I. Peterson, J. Heptinstall, D.J. Walton, Biosens. Bioelectron. **14**, 265 (1999)
M. Dawgul, D.G. Pijanowska, A. Krzyskow, J. Kruk, W. Torbicz, Sensors **3**, 146 (2003)
M. Dimaki, M. Vergani, A. Heiskanen, D. Kwasny, L. Sasso, M. Carminati, J. Gerrard, J. Emneus, W.E. Svendsen, Sensors **14**, 9505 (2014)
S. Goennenwein, M. Tanaka, B. Hu, L. Moroder, E. Sackmann, Biophys. J. **85**, 646 (2003)
J.-G. Guan, Y.-Q. Miao, Q.-J. Zhang, J. Biosci. Bioeng. **97**, 219 (2004)
R. Guidelli, G. Aloisi, L. Becucci, A. Dolfi, M. Rosa Moncelli, F. Tadini Buoninsegni, J. Electroanal. Chem. **504**, 1 (2001)
J. S. Hansen, M. Perry, J. Vogel, T. Vissing, C. R. Hansen, O. Geschke, J. Emnéus, and C. H. Nielsen, J. Micromech. Microeng. **19**, 025014 (11pp) (2009)
A.R. Heiskanen, C.F. Spégel, N. Kostesha, T. Ruzgas, J. Emnéus, Langmuir **24**, 9066 (2008)
M. Hetzer, S. Heinz, S. Grage, and T. M. Bayerl, **7463**, 982 (1998)
B. Hirschorn, M.E. Orazem, B. Tribollet, V. Vivier, I. Frateur, M. Musiani, Electrochim. Acta **55**, 6218 (2010)
N. Inagaki, K. Narushima, S.K. Lim, Y.W. Park, Y. Ikeda, J. Polym. Sci. B Polym. Phys. **40**, 2871 (2002)
B. Kelety, K. Diekert, J. Tobien, N. Watzke, W. Dörner, P. Obrdlik, K. Fendler, Assay. Drug. Dev. Technol. **4**, 575 (2006)
A. Kibrom, R.F. Roskamp, U. Jonas, B. Menges, W. Knoll, H. Paulsen, R.L.C. Naumann, Soft Matter **7**, 237 (2011)
Y.-R. Kim, S. Jung, H. Ryu, Y.-E. Yoo, S.M. Kim, T.-J. Jeon, Sensors **12**, 9530 (2012)
W. Knoll, I. Köper, R. Naumann, E.-K. Sinner, Electrochim. Acta **53**, 6680 (2008)
M. Kühner, R. Tampé, E. Sackmann, Biophys. J. **67**, 217 (1994)
J. Leitch, J. Kunze, J.D. Goddard, A.L. Schwan, R.J. Faragher, R. Naumann, W. Knoll, J.R. Dutcher, J. Lipkowski, Langmuir **25**, 10354 (2009)
J. Lipkowski, Phys. Chem. Chem. Phys. **12**, 13874 (2010)
T.M. Long, S. Prakash, M.A. Shannon, J.S. Moore, Langmuir **22**, 4104 (2006)
J.T. Marquês, R.F.M. de Almeida, A.S. Viana, Soft Matter **8**, 2007 (2012)
I.P. Mccabe, M.B. Forstner, Open. J. Biophys. **3**, 59 (2013)
A. Michalke, T. Schürholz, H.-J. Galla, C. Steinem, Langmuir **17**, 2251 (2001)
W.C. Mueller, P. Rudin, D.O. Tien, H.T. Wescott, Nature **194**, 979 (1962)
R. Naumann, D. Walz, S. M. Schiller, and W. Knoll, J. Electroanal. Chem. **550-551**, 241 (2003)
C.H. Nielsen, Anal. Bioanal. Chem. **395**, 697 (2009)
A.L. Plant, Langmuir **9**, 2764 (1993)
R.S. Ries, H. Choi, R. Blunck, F. Bezanilla, J.R. Heath, J. Phys. Chem. B **108**, 16040 (2004)
R. Robelek, E.S. Lemker, B. Wiltschi, V. Kirste, R. Naumann, D. Oesterhelt, E.-K. Sinner, Angew. Chem. Int. Ed. **46**, 605 (2007)
M. Roerdink Lander, S. Ibragimova, C. Rein, J. Vogel, K. Stibius, O. Geschke, M. Perry, C. Hélix-Nielsen, Langmuir **27**, 7002 (2011)
E. Sackmann, Science. **271**(80), 43 (1996)

A. Samide, A. Ciuciu, C. Negrila, Port. Electrochim. Acta **28**, 385 (2010)
M.L. Steen, C.I. Butoi, E.R. Fisher, Langmuir **17**, 8156 (2001)
C. Steinem, A. Janshoff, H.-J. Galla, M. Sieber, Bioelectrochem. Bioenerg. **42**, 213 (1997)
M.M. Sung, G.J. Kluth, R. Maboudian, J. Vac. Sci. Technol. A **17**, 540 (1999)
L.K. Tamm, H.M. McConnell, Biophys. J. **47**, 105 (1985)
M. Tanaka, E. Sackmann, Nature **437**, 656 (2005)
B.D. Tompkins, J.M. Dennison, E.R. Fisher, J. Membr. Sci. **428**, 576 (2013)
A. Ulman, Chem. Rev. **96**, 1533 (1996)
J. Vidič, A. Podgornik, A. Štrancar, J. Chromatogr. A **1065**, 51 (2005)
A. Wardak, H.T. Tien, Bioelectrochem. Bioenerg. **24**, 1 (1990)
C.-S. Wu, M.K.K. Oo, J.M. Cupps, X. Fan, Biosens. Bioelectron. **26**, 3870 (2011)
M. Zagnoni, Lab Chip **12**, 1026 (2012)